



Cite this: *Nanoscale*, 2017, **9**, 17983

## A two-dimensional TiB<sub>4</sub> monolayer exhibits planar octacoordinate Ti<sup>†</sup>

Xin Qu,<sup>a</sup> Jinghai Yang,<sup>a,\*e</sup> Yanchao Wang,<sup>c,d</sup> Jian Lv,<sup>\*c</sup> Zhongfang Chen<sup>f</sup> and Yanming Ma<sup>d</sup>

At present, the concept of planar hypercoordination in chemistry meets the fast development of two-dimensional (2D) nanomaterials, leading to considerable interest in searching for 2D materials with planar hypercoordinate atoms. In this work, by means of the swarm-intelligence structure search method and first-principles calculations, we predict a hitherto unknown 2D TiB<sub>4</sub> monolayer with a planar octacoordinate Ti moiety, in which each Ti atom binds to eight B atoms with equal distances in a perfect plane, and has the highest coordination of Ti known for 2D materials thus far. Systematic *ab initio* calculations demonstrate the superior thermodynamic and dynamic stabilities of the predicted TiB<sub>4</sub> monolayer, indicating the high feasibility for experimental synthesis. The stabilization of this perfect planar structure originates from the geometric fit between the atomic radius of Ti and the size of the 8-membered B ring, as well as the electron transfer from Ti to B atoms which compensates the electron deficiency of the full sp<sup>2</sup> hybridized B network. Motivated by the unforeseen geometry of the TiB<sub>4</sub> monolayer, a series of other 2D transition metal borides (TMB<sub>4</sub>, TM = V, Cr, Mo, W and Os) with quasi-planar octacoordinate TM atoms are further designed and discussed. The present work provides a useful roadmap for the discovery of 2D hypercoordinate materials.

Received 2nd August 2017,  
Accepted 25th October 2017

DOI: 10.1039/c7nr05688e

rsc.li/nanoscale

## 1. Introduction

The establishment of the concept of planar hypercoordination in molecules is an important advancement in chemistry over the last 40 years.<sup>1–3</sup> In 1970, the seminal work by Hoffmann challenged the tetrahedral configuration of carbon by proposing a σ-donor and π-acceptor strategy to stabilize planar tetra-coordinate carbon (ptC).<sup>4</sup> Based on this electronic stabilization strategy, Schleyer and coworkers theoretically designed the first ptC-containing molecule, 1,1-dilithiocyclopropane, in 1976.<sup>5</sup> Ever since, research interest in searching for ptC-containing species has been ignited,<sup>6</sup> and numerous ptC-contain-

ing molecules/clusters, such as CAI<sub>4</sub><sup>–</sup>,<sup>7</sup> CAI<sub>4</sub><sup>2–</sup>,<sup>8</sup> and CAI<sub>3</sub>Si<sup>–</sup>,<sup>9</sup> have been theoretically designed and/or experimentally realized. More interestingly, Schleyer and coworkers further extended this concept to molecules/clusters with even higher coordination numbers of carbon in a planar environment;<sup>10–12</sup> many more molecules/clusters containing planar pentacoordinate carbon (ppC),<sup>11,13–17</sup> planar hexacoordinate carbon (phC)<sup>18,19</sup> and even planar heptacoordinate carbon<sup>11,20</sup> have been identified theoretically.

The concept of planar hypercoordination has also been extended to elements other than carbon. A number of species with planar hypercoordination of the main group elements, such as boron,<sup>21,22</sup> nitrogen,<sup>23–26</sup> oxygen,<sup>27,28</sup> sulfur,<sup>29</sup> silicon,<sup>30</sup> germanium,<sup>31</sup> phosphorus<sup>32</sup> and arsenic,<sup>33</sup> have been theoretically and/or experimentally achieved. Strikingly, inspired by the discovery of planar hepta- and octacoordinate B in wheel-type geometries of B<sub>8</sub><sup>2–</sup> and B<sub>9</sub><sup>–</sup> clusters,<sup>21</sup> a team led by Wang and Boldyrev realized a series of transition-metal-centered borometallic molecular wheels: FeB<sub>8</sub><sup>–</sup>,<sup>34</sup> FeB<sub>9</sub><sup>–</sup>,<sup>34</sup> CoB<sub>8</sub><sup>–</sup>,<sup>35</sup> RuB<sub>9</sub><sup>–</sup>,<sup>35</sup> RhB<sub>9</sub>,<sup>36</sup> IrB<sub>9</sub>,<sup>36</sup> NbB<sub>10</sub><sup>–</sup><sup>37</sup> and TaB<sub>10</sub><sup>–</sup>,<sup>37</sup> among which NbB<sub>10</sub><sup>–</sup> and TaB<sub>10</sub><sup>–</sup> hold the highest planar coordination numbers thus far.<sup>38</sup> All these achievements have significantly enriched the planar hypercoordination chemistry.

Planar hypercoordinate configurations are not found in isolated molecules/clusters only. The exotic geometries along with rule-breaking chemical bonding also stimulated research-

<sup>a</sup>Changchun Institute of Optics, Fine Mechanics and Physics, Chinese Academy of Sciences, Changchun 130033, P. R. China

<sup>b</sup>University of Chinese Academy of Sciences, Beijing 100039, P. R. China

<sup>c</sup>College of Materials Science and Engineering, Jilin University, Changchun 130012, China. E-mail: lvjian@calypso.cn

<sup>d</sup>State Key Laboratory of Superhard Materials, College of Physics, Jilin University, Changchun 130012, China

<sup>e</sup>Key Laboratory of Functional Materials Physics and Chemistry of the Ministry of Education, Jilin Normal University, Changchun 130103, PR China.

E-mail: jhyang1@jlnu.edu.cn

<sup>f</sup>Department of Chemistry, University of Puerto Rico, Rio Piedras Campus, San Juan, Puerto Rico 00931, USA

<sup>†</sup>Electronic supplementary information (ESI) available. See DOI: 10.1039/c7nr05688e

ers to explore their viability in extended systems. Based on the previously proposed ptC fragment  $C_5^{2-}$ ,<sup>39,40</sup> Hoffmann and coworkers designed several ptC-containing three-dimensional (3D) networks with the stoichiometry of  $C_5M_x$  ( $M = Li$ ,  $x = 2$ ;  $M = Be, Pt, Zn$ ,  $x = 1$ ).<sup>41</sup> At present, the planar coordination chemistry meets the rapid development of 2D graphene-like materials. A number of 2D monolayers with planar hypercoordinate motifs have been designed. For example, Wu *et al.*<sup>42</sup> theoretically designed  $CB_2$  graphene with a ptC moiety based on the ptC molecule  $CB_4$ . A global structure search for 2D  $B_xC_y$  compounds by Luo *et al.*<sup>43</sup> revealed several ptC-containing monolayers including  $B_2C$ ,  $B_3C$ , and  $B_5C$ . Zhang *et al.*<sup>44</sup> proposed a tetragonal TiC monolayer fully composed of quasi-planar tetracoordinate carbons with orientation-dependent electronic properties. Li *et al.*<sup>45</sup> and Dai *et al.*<sup>46</sup> discovered ptC-containing monolayers in the Al–C system independently, and Liu *et al.*<sup>47</sup> found the ptC motif in a BeC monolayer. Furthermore, ppC- and phC-containing monolayers were also identified in  $Be_2C$  and  $Be_3C_2$ ,<sup>48,49</sup> respectively. Besides carbon, the planar or quasi-planar hypercoordinate configuration of heavier group 14 congeners, *e.g.* Si and Ge, as well as noble metal elements were also uncovered in 2D materials, such as  $SiC_2$ ,<sup>50</sup>  $Cu_2Ge$ ,<sup>51</sup>  $Cu_2Si$ ,<sup>52</sup>  $Ni_2Si$ ,<sup>53</sup> and  $Ni_2Ge$ ,<sup>53</sup> among which planar hexacoordinate Cu and Si/Ge can be stabilized simultaneously in  $Cu_2Si/Ge$  monolayers.<sup>52,52</sup> Strikingly, the first example with a planar hypercoordinate transition metal (TM) moiety in 2D materials has been recently uncovered in  $FeB_6$  monolayers with quasi-planar octacoordinate or planar hexacoordinate Fe.<sup>54</sup> With exotic geometries, rule-breaking chemical bonding, appealing mechanical and electronic properties, these 2D hypercoordinate materials are not only attractive to fundamental science but also promising candidates for application in electronics, optoelectronics and photovoltaics.

Compared with various planar hypercoordinate TM motifs discovered in isolated borometallic molecular wheels with coordination numbers up to 10,<sup>55</sup> the corresponding findings in 2D materials are rather rare. Moreover, the only examples such as  $TiB_2$ ,<sup>56</sup>  $FeB_2$ <sup>57</sup> and  $FeB_6$ <sup>54</sup> monolayers are with quasi-planar configurations. Given that possible chemical compositions of transition metal borides are much broader than what have been explored so far, one would wonder if there exist other TM atoms that can be stabilized in 2D space as hypercoordinate motifs.

In this work, through the intensive swarm-intelligent global structure search method combined with first-principles calculations, we predict a new 2D material, namely the  $TiB_4$  monolayer, which consists of edge-sharing  $Ti@B_8$  wheels with planar octacoordinate Ti atoms located at the center of 8-membered B rings. The predicted  $TiB_4$  monolayer is stabilized within a pure plane and is the energetically most favourable configuration in 2D space. It has relatively good thermodynamic and dynamic stabilities, which is attributed to the electron transfer from Ti to the B network as well as a geometric fit between the atomic radius of Ti and the size of the B rings. Based on the novel  $TiB_4$  monolayer, we further proposed a series of 2D materials

with quasi-planar octacoordinate TM motifs in the stoichiometry of  $TMB_4$ , where  $TM = V, Cr, Mo, W$  and  $Os$ .

## 2. Computational details

The search for structures of the  $TiB_4$  system was based on the global minimization of free energy surfaces using *ab initio* total energy calculations and the particle-swarm-optimization scheme as implemented in the CALYPSO code.<sup>43,58–60</sup> Several techniques are included in the algorithm to improve the search efficiency, *e.g.* 2D space group symmetry constraints in structural generation, a bond characterization matrix technique for fingerprinting structures, local version of the PSO algorithm enabling a simultaneous search in different energy funnels, *etc.* Its validity has been manifested by successful identification of the ground-state structures for a large number of systems.<sup>47,49,54,61–65</sup> During the search for structures, both planar and buckled structures were considered. The population size was set as 200, and the number of generations was maintained at 10. Simulation cells containing 1, 2, 3, 4 and 8 formula units were considered for  $TiB_4$ , while 2, 3 and 4 formula units were considered for other TM borides.

The underlying energy calculations and structure optimizations were performed in the framework of density functional theory using the Vienna *ab initio* simulation package.<sup>66</sup> The projector-augmented plane wave (PAW)<sup>67</sup> approach was used to represent the ion–electron interaction. The electron exchange–correlation functional was treated using the generalized gradient approximation proposed by Perdew, Burke and Ernzerhof (PBE).<sup>68</sup> The energy cutoff of the plane wave was set to be 650 eV with the energy precision of  $10^{-6}$  eV. The atomic positions were fully relaxed until the maximum force on each atom was less than  $10^{-3}$  eV  $\text{\AA}^{-1}$ . The van der Waals (vdW) correction proposed by Becke (optB88-vdW)<sup>69</sup> was chosen to describe the long-range interaction for double-layer structures. The Brillouin zone was sampled with a  $12 \times 12 \times 1$   $\Gamma$ -centered Monkhorst–Pack  $k$ -point grid for geometry optimization and self-consistent calculations. 2D monolayers were placed in the  $xy$  plane with the  $z$  direction perpendicular to the layer plane, and a vacuum space of 20  $\text{\AA}$  in the  $z$  direction was adopted to avoid interactions between the adjacent layers.

Phonon calculations were carried out using the frozen phonon approach as implemented in the PHONOPY package.<sup>70</sup> *Ab initio* molecular dynamics (AIMD) simulations using the PAW method and the PBE functional were performed at different temperatures up to 3000 K to evaluate the thermal stability of the  $TiB_4$  monolayer. The initial configuration was taken from the optimized structure at zero temperature with a  $3 \times 3$  supercell (9 Ti atoms and 36 B atoms). Each AIMD simulation in the NVT ensemble lasted for 40 ps with a time step of 2.0 fs, and the temperature was controlled by using the Nosé–Hoover method.<sup>71</sup> The Visualization for Electronic and Structural Analysis software (VESTA 3)<sup>72</sup> was used for visualization and plotting.

### 3. Results and discussion

#### 3.1 Geometric structure of the TiB<sub>4</sub> monolayer

The recently proposed TiB<sub>2</sub> monolayer, Dirac material, has a large vertical distance of 1.19 Å between Ti and the honeycomb B network, implying that Ti is too large to be embedded into the B hexagon.<sup>56</sup> It motivated us to investigate Ti–B systems with a higher B concentration (e.g. TiB<sub>4</sub>) to achieve 2D monolayers with higher planar coordination numbers. Interestingly, structure predictions for 2D TiB<sub>4</sub> by the CALYPSO method revealed that a completely planar structure with octacoordinate Ti atoms has the lowest energy, and thus a global minimum in 2D space (Fig. 1, other low-lying isomers are given in Fig. S1 in the ESI†). Within this global minimum structure (Fig. 1), each Ti atom is octacoordinated to B atoms with an equal Ti–B bond length of 2.22 Å, and the B atoms form a network composed of 4-membered and 8-membered rings. The structure can be constructed using the motif of Ti@B<sub>8</sub> wheels, which connect each other by sharing B–B edges or forming B squares. One unit cell of the TiB<sub>4</sub> monolayer contains one Ti atom and four B atoms with the optimized lattice constants of  $a = b = 4.11$  Å. The B–B bond length in B squares is 1.72 Å, a little longer than those shared by the Ti@B<sub>8</sub> wheels (1.68 Å). All the Ti–B and B–B bond lengths are smaller than those in the bulk TiB<sub>2</sub><sup>73</sup> (2.38 and 1.75 Å for Ti–B and B–B bond lengths, respectively), indicating much stronger interactions within the TiB<sub>4</sub> monolayer. We also considered several buckled configurations as potential ground-state TiB<sub>4</sub> monolayers by displacing Ti and/or B atoms along the out-of-plane direction by a small distance. The distorted structures spontaneously transform into a pure plane upon geometry optimization,

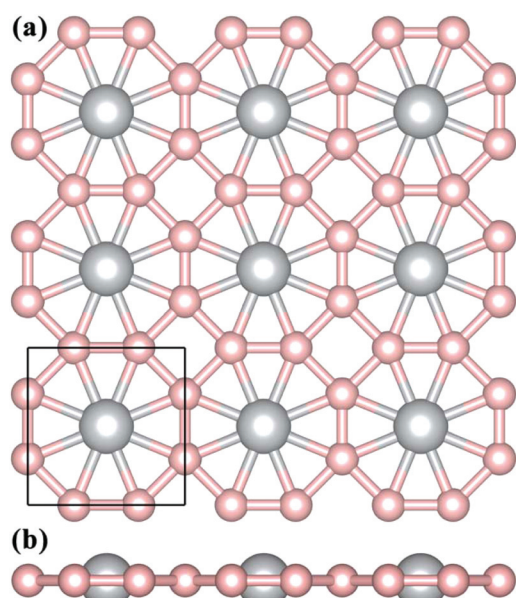


**Fig. 1** (a) Top and (b) side views of the ball and stick model of the predicted 2D TiB<sub>4</sub> monolayer. Ti and B atoms are denoted by grey and pink spheres, respectively. The black square marks a unit cell. The Ti atoms are located at the center of octagonal B rings.

implying the robustness of the planar geometry. Considering the large vertical distance in a previously proposed TiB<sub>2</sub> monolayer, the geometric fit between the atomic radius of Ti and the size of the 8-membered B rings is responsible for the stabilization of the purely planar geometry in the TiB<sub>4</sub> monolayer. To the best of our knowledge, the TiB<sub>4</sub> monolayer is the first example of a 2D graphene-like material containing completely planar octacoordinate TM atoms.

#### 3.2 Stability of the TiB<sub>4</sub> monolayer

To evaluate the stability of this newly predicted TiB<sub>4</sub> monolayer, we first computed its cohesive energy,  $E_{\text{coh}} = (xE_{\text{Ti}} + 4xE_{\text{B}} - xE_{\text{TiB}_4})/5x$ , where  $E_{\text{Ti}}$ ,  $E_{\text{B}}$  and  $E_{\text{TiB}_4}$  are the total energies of a single Ti atom, a single B atom, and one unit cell of the TiB<sub>4</sub> monolayer, respectively. The TiB<sub>4</sub> monolayer has a cohesive energy of 6.42 eV per atom, higher than that of Fe–B (5.79–4.87 eV per atom),<sup>54,57</sup> Be–C (4.82–4.58 eV per atom)<sup>47,49,74</sup> and Cu<sub>2</sub>Si (3.46 eV per atom)<sup>52</sup> monolayers at the same theoretical level, indicating that it is a strongly bonded network.

No imaginary frequency in the first Brillouin zone (Fig. S2 in the ESI†) was found in the phonon dispersion calculations, which confirms the dynamic stability of the TiB<sub>4</sub> monolayer. The highest frequency of the TiB<sub>4</sub> monolayer reaches up to 1105 cm<sup>-1</sup>, which is in the same order of magnitude as the recently proposed FeB<sub>6</sub> (1316 cm<sup>-1</sup>)<sup>54</sup> and Be<sub>5</sub>C<sub>2</sub> (1120 cm<sup>-1</sup>)<sup>49</sup> monolayers, and higher than those of FeB<sub>2</sub> (854 cm<sup>-1</sup>),<sup>57</sup> TiC (810 cm<sup>-1</sup>),<sup>44</sup> Cu<sub>2</sub>Si (420 cm<sup>-1</sup>)<sup>52</sup> and MoS<sub>2</sub> (473 cm<sup>-1</sup>)<sup>75</sup> monolayers. The high value of frequencies in the phonon spectra also indicates the robust interactions in our newly predicted TiB<sub>4</sub> monolayer.

Furthermore, to evaluate the thermal stability, we carried out AIMD simulations for the TiB<sub>4</sub> monolayer with a 3 × 3 supercell at different temperatures of 500, 1000, 1500, 2000, 2500 and 3000 K. The snapshots of the TiB<sub>4</sub> monolayer taken at the end of 40 ps simulation are shown in Fig. 2 (the temperature/energy fluctuations *versus* simulation time is given in Fig. S3 in the ESI†). The original geometry of the TiB<sub>4</sub> monolayer is generally well maintained with only slight in-plane and out-of-plane deformations up to 2500 K. The distorted structures can restore the planar structure after geometry optimization. As the temperature increases, the distortions become more and more pronounced, and the framework of the TiB<sub>4</sub> monolayer collapses at an extremely high temperature of 3000 K. The well-preserved geometry of the TiB<sub>4</sub> monolayer at such a high temperature of up to 2500 K indicates its remarkable thermal stability and possible application at high temperatures. Simulations based on larger 4 × 4 supercells give consistent results as those obtained using 3 × 3 supercells. It is really remarkable that this 2D monolayer can resist such a high temperature of 2500 K.

What about the interlayer interaction energies when the individual TiB<sub>4</sub> monolayers are stacked together? To address this question, we investigated various types of double-layer stackings of TiB<sub>4</sub> monolayers, and found that the stacking with upper-layer Ti atoms located above the center of the 4-membered B rings in the sublayer is most favourable energetically

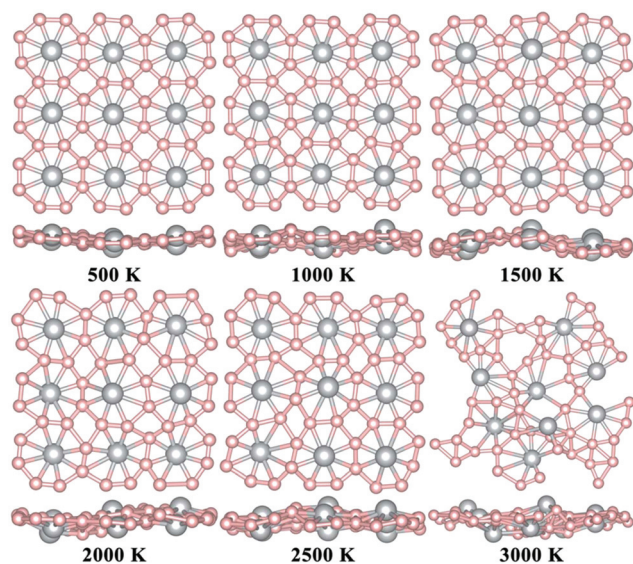


Fig. 2 Snapshots of the final frame of the  $\text{TiB}_4$  monolayer at temperatures from 500 to 3000 K (top and side views) at the end of 40 ps molecular dynamics (MD) simulations.

(for detailed structural information, refer to Fig. S4(a) and (b) in the ESI†). The vertical interlayer distance between the B–B layers is 2.78 Å. The calculated interlayer interaction energy is 351 meV per atom, indicating a moderate interaction between the layers. However, ELF plot (Fig. S4(c)†) indicates that there is no obvious electron localization between the layers. Therefore, both van der Waals and ionic interactions are responsible for the interlayer interactions.

Considering the moderate interlayer binding energy and that no layered bulk material of our newly predicted  $\text{TiB}_4$  monolayer is available, it is not possible to obtain  $\text{TiB}_4$  monolayers by the widely used exfoliation method. However, this cannot rule out their experimental realization. It is known that single-layer borophene<sup>76–78</sup> and silicene<sup>79</sup> have already been synthesized on metal substrates, though they also do not have layered bulk counterparts.

### 3.3 Electronic properties and stabilization mechanism

To gain deep insight into the chemical bonding nature of the  $\text{TiB}_4$  monolayer, we calculated the electron localization function (ELF) to analyse its electron distributions. The ELF, defined to have the convenient range of values between 0 and 1, is known to be an informative tool to distinguish different bonding interactions in molecules or solids.<sup>80</sup> The regions in which the ELF value is close to 0.5 or 1.0 correspond to a perfect free-electron gas distribution or well-localized electrons, respectively. As shown in Fig. 3(a), the isosurface of ELF with a value of 0.75 shows substantial accumulation of electrons at the middle of the B–B bonds, denoting strong interactions within the B network through two-center two-electron B–B  $\sigma$  bonds. Moreover the ELF map in the (001) section through the  $\text{TiB}_4$  monolayer (Fig. 3(b)) shows that the blue color corresponding to the ELF value of 0 is mainly around Ti

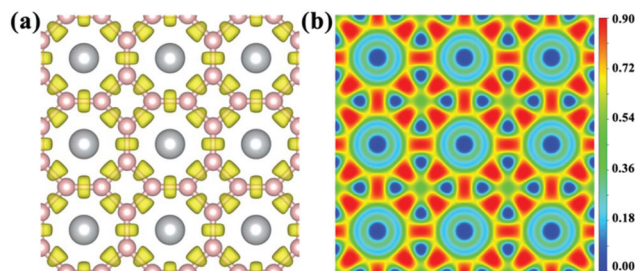


Fig. 3 Isosurface of ELF plotted with a value of 0.75 (a) and the ELF map sliced perpendicular to the (001) direction (b) for the  $\text{TiB}_4$  monolayer. In the ELF map, the red and blue colors refer to the highest (0.90) and the lowest values (0.00) of ELF.

atoms. This indicates the electron deficiency of Ti and electron transfer from Ti to the B network. Since no significant electron localization can be found between Ti and B in the ELF map, the interactions between Ti and the B network are predominantly ionic. The deformation electronic density (DED), which is defined as the electron density of the  $\text{TiB}_4$  monolayer minus the superposition of the isolated atomic densities, generally gives consistent results as that of ELF (Fig. S5 in the ESI†). The Bader charge analysis<sup>81</sup> shows that each Ti transfers  $\sim 1.67e$  to the B network.

To further understand the stabilization mechanism, we calculated the electronic band structure and the projected density of states (PDOS) of the  $\text{TiB}_4$  monolayer as well as the PDOS of the bare B network in the  $\text{TiB}_4$  monolayer (Fig. 4). The band

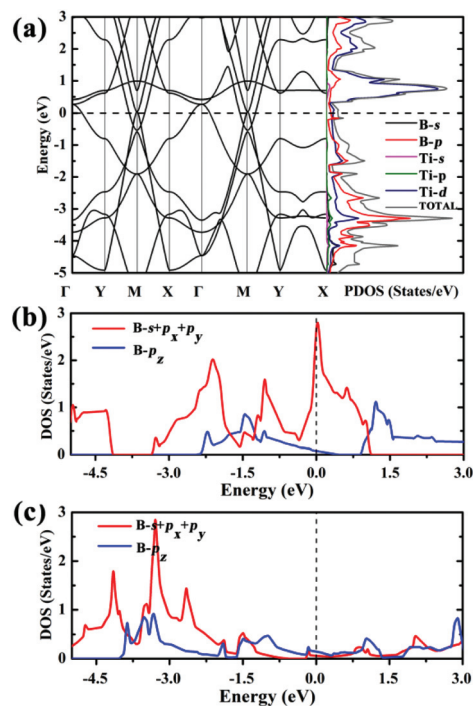


Fig. 4 (a) Electronic band structure and PDOS of the  $\text{TiB}_4$  monolayer, PDOS presents the in-planar B-s +  $p_x$  +  $p_y$  and out-of-plane B- $p_z$  states for (b) the bare B network and (c) the  $\text{TiB}_4$  monolayer.

structure and PDOS shown in Fig. 4(a) show that the TiB<sub>4</sub> monolayer is metallic with several bands across the Fermi level. The conduction bands are mainly dominated by the Ti-d states, while the valence bands are predominantly composed of B-p and Ti-d states with strong hybridization. Note that within the B network of the TiB<sub>4</sub> monolayer, each B atom is coordinated to three other B atoms, featuring sp<sup>2</sup> hybridization similar to that in graphene with a honeycomb structure. But due to the electron deficient nature of the B atom, a bare B network with fully sp<sup>2</sup> hybridization could not be stable. This is evident from the PDOS of the bare B network (Fig. 4(b)), where substantial in-plane sp<sup>2</sup> bonding states (B-s, B-p<sub>x</sub> and B-p<sub>y</sub> states) are unoccupied with a high peak located at the Fermi level. However, when Ti atoms are embedded into the 8-membered B rings, electron transfer from Ti to B atoms compensates for this electron deficiency, which leads to almost fully occupied in-plane sp<sup>2</sup> bonding states, placing the Fermi level within the gap between the in-plane bonding and anti-bonding states (Fig. 4(c)). Thus the fully sp<sup>2</sup> hybridized B network is electronically stabilized in the TiB<sub>4</sub> monolayer.

### 3.4 Absorption and diffusion of lithium on the TiB<sub>4</sub> monolayer

The intrinsic metallicity of the TiB<sub>4</sub> monolayer makes it a promising anode material for Li-ion batteries (LIBs).<sup>82,83</sup> Therefore, we explored the adsorption and diffusion of lithium on the TiB<sub>4</sub> monolayer by evaluating the adsorption energy and the diffusion energy barrier. We first selected some inequivalent high-symmetry adsorption sites, then deposited a single Li atom on each adsorption site of a 3 × 3 supercell. Geometry optimizations indicate that the most favourable Li adsorption site resides on the top of the four-membered B rings, and the binding energy is −1.04 eV. Then, we performed standard nudged elastic band (NEB)<sup>84</sup> calculations to evaluate the mobility of Li atoms on the TiB<sub>4</sub> monolayer. Although it is impossible for Li to penetrate the layer, as indicated by the extremely high energy barrier of 5.37 eV (see Fig. S6 in the ESI† for details), Li diffusion between two most favourable adsorption sites on the same side of the TiB<sub>4</sub> monolayer (Fig. 5) is rather facile. It only needs to overcome a small energy barrier of 0.18 eV, which is smaller than that on single-

layer silicene (0.23 eV).<sup>85</sup> Another pathway between two favourable adsorption sites on the same side of the TiB<sub>4</sub> monolayer (Fig. S7 in the ESI†) also has a small energy barrier of 0.24 eV. The small energy barrier of in-plane Li diffusion will lead to a good Li ion conductivity.

Next, we explored the Li storage capacity of the TiB<sub>4</sub> monolayer by evaluating the binding energy of a number of configurations with the stoichiometry of Li<sub>x</sub>TiB<sub>4</sub> (x = 2, 4, 6). Encouragingly, the TiB<sub>4</sub> monolayer can provide a negative Li binding energy (−0.46 eV) even at x = 2, indicating that Li atoms can still be stably adsorbed on the TiB<sub>4</sub> monolayer and the phase separation problem can be safely avoided at such a high concentration. As Li<sub>2</sub>TiB<sub>4</sub> represents the highest Li storage capacity, we can easily deduce that the TiB<sub>4</sub> monolayer has a theoretical capacity of 588 mA h g<sup>−1</sup>. We then computed the average open circuit voltage (OCV) for Li intercalation on the TiB<sub>4</sub> monolayer. The OCV for Li intercalation in the TiB<sub>4</sub> monolayer can be computed from the energy difference based on the equation below:<sup>82</sup>

$$\text{OCV} \approx [E_{\text{Li}_x\text{TiB}_4} - E_{\text{Li}_{x-1}\text{TiB}_4} + (x_2 - x_1)E_{\text{Li}}]/(x_2 - x_1)e$$

where  $E_{\text{Li}_x\text{TiB}_4}$ ,  $E_{\text{Li}_{x-1}\text{TiB}_4}$ , and  $E_{\text{Li}}$  are the total energies of Li<sub>x</sub>TiB<sub>4</sub>, Li<sub>x−1</sub>TiB<sub>4</sub>, and metallic Li, respectively. According to this equation, when the TiB<sub>4</sub> monolayer reaches the highest Li capacity, corresponding to the case of x = 2 in Li<sub>2</sub>TiB<sub>4</sub>, the computed average OCV is 0.23 V, which is between those of the commercial anode materials, 0.11 V for graphite and 1.5–1.8 V for TiO<sub>2</sub>.<sup>82</sup> Overall, the small diffusion energy barrier along with high Li storage capacity and applicable OCV provide significant feasibility for TiB<sub>4</sub> monolayers to be used as LIB anodes.

### 3.5 Other TMB<sub>4</sub> monolayers with quasi-planar octacoordinate TM motifs

Motivated by the novel planar geometry of the TiB<sub>4</sub> monolayer, we further accessed its viability in other TM borides with the stoichiometry of TMB<sub>4</sub>. By substituting the Ti atom in the TiB<sub>4</sub> monolayer with other TM atoms and subsequent geometry optimizations, we found that the planar geometry can be maintained in TMB<sub>4</sub> monolayers for TM = V, Cr, Mo, W and Os. Unfortunately, the search for the global structure of these

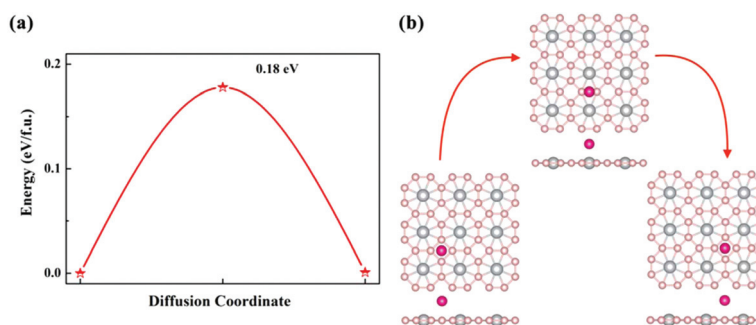


Fig. 5 Pathways for the diffusion of Li on the TiB<sub>4</sub> monolayer. (a) The variation of energy (red solid line) is plotted along the diffusion coordinates. The energy maximum (corresponding to the barrier value of 0.18 eV) is indicated. (b) Initial, middle and final configurations of the diffusion pathway.

TMB<sub>4</sub> (TM = V, Cr, Mo, W and Os) monolayers revealed that the buckled structures are energetically more stable than the planar ones, thus ruling out the existence of the completely planar geometry in other TM borides.

Fig. S8† presents the lowest-energy structures of TMB<sub>4</sub> (TM = V, Cr, Mo, W and Os) monolayers revealed by CALYPSO. All of them possess a quasi-planar geometry, in which each TM atom is coordinated to eight B atoms, forming quasi-planar octacoordinate TM moieties. Interestingly, all these structures exhibit a similar geometric topology as that of the TiB<sub>4</sub> monolayer, e.g. TM@B<sub>8</sub> wheels connecting each other by sharing B–B edges or forming four-membered B rings. A similar geometry topology of these TMB<sub>4</sub> monolayers further highlights the special role of Ti in the stabilization of the novel planar structures. Further investigation on the detailed properties of these quasi-planar TMB<sub>4</sub> monolayers is beyond the scope of the present work, but is underway.

## 4. Conclusions

In summary, by means of first-principles calculations and the swarm-intelligence structure search method, we identified a completely planar graphene-like material containing octacoordinate Ti motifs, namely the TiB<sub>4</sub> monolayer, as the global minimum in 2D space. This novel planar structure possesses superior thermodynamic, dynamic and thermal stabilities. The coincidence of geometric and electronic fits is responsible for the stabilization of this exotic planar structure. Further structure search calculations rule out the existence of the completely planar structure for other TMB<sub>4</sub> monolayers, but revealed a series of buckled structures with quasi-planar octacoordinate motifs in VB<sub>4</sub>, CrB<sub>4</sub>, MoB<sub>4</sub>, WB<sub>4</sub> and OsB<sub>4</sub>, which highlight the unique role of the Ti atom in stabilizing this planar structure. To the best of our knowledge, this is the first example of a 2D graphene-like material containing completely planar octacoordinate TM atoms. Note that with reasonable choices of transition metal atoms and the appropriate number of B atoms, other planar structures with hypercoordinate TM atoms are also likely to be stabilized. Thus, this finding is paving the way for the discovery of more 2D hypercoordinate materials.

## Conflicts of interest

There are no conflicts to declare.

## Acknowledgements

The authors acknowledge financial support from the National Natural Science Foundation of China (Grants No. 11534003, 11604117, 11404128 and 61775081), the Science Challenge Project (No. TZ2016001), the National Key Research and Development Program of China (Grant No. 2016YFB0201200 and 2017YFF0108607), and the Program for JLU Science and

Technology Innovative Research Team. Part of the calculations was performed in the high performance computing center of Jilin University and Tianhe2-JK in the Beijing Computational Science Research Center.

## References

- 1 R. Keese, *Chem. Rev.*, 2006, **106**, 4787–4808.
- 2 W. Siebert and A. Gunale, *Chem. Soc. Rev.*, 1999, **28**, 367–371.
- 3 L.-M. Yang, E. Ganz, Z. Chen, Z.-X. Wang and P. V. R. Schleyer, *Angew. Chem., Int. Ed.*, 2015, **54**, 9468–9501.
- 4 R. Hoffmann, R. W. Alder and C. F. Wilcox, *J. Am. Chem. Soc.*, 1970, **92**, 4992–4993.
- 5 J. B. Collins, J. D. Dill, E. D. Jemmis, Y. Apeloig, P. V. R. Schleyer, R. Seeger and J. A. Pople, *J. Am. Chem. Soc.*, 1976, **98**, 5419–5427.
- 6 G. Merino, M. A. Méndez-Rojas, A. Vela and T. Heine, *J. Comput. Chem.*, 2007, **28**, 362–372.
- 7 X. Li, L.-S. Wang, A. I. Boldyrev and J. Simons, *J. Am. Chem. Soc.*, 1999, **121**, 6033–6038.
- 8 X. Li, H.-F. Zhang, L.-S. Wang, G. D. Geske and A. I. Boldyrev, *Angew. Chem., Int. Ed.*, 2000, **39**, 3630–3632.
- 9 L.-S. Wang, A. I. Boldyrev, X. Li and J. Simons, *J. Am. Chem. Soc.*, 2000, **122**, 7681–7687.
- 10 K. Exner, *Science*, 2000, **290**, 1937–1940.
- 11 Z.-X. Wang, *Science*, 2001, **292**, 2465–2469.
- 12 R. Islas, T. Heine, K. Ito, P. V. R. Schleyer and G. Merino, *J. Am. Chem. Soc.*, 2007, **129**, 14767–14774.
- 13 Y. Pei, W. An, K. Ito, P. V. R. Schleyer and X. C. Zeng, *J. Am. Chem. Soc.*, 2008, **130**, 10394–10400.
- 14 J. O. C. Jimenez-Halla, Y.-B. Wu, Z.-X. Wang, R. Islas, T. Heine and G. Merino, *Chem. Commun.*, 2010, **46**, 8776.
- 15 R. Grande-Aztatzi, J. L. Cabellos, R. Islas, I. Infante, J. M. Mercero, A. Restrepo and G. Merino, *Phys. Chem. Chem. Phys.*, 2015, **17**, 4620–4624.
- 16 A. C. Castro, G. Martínez-Guajardo, T. Johnson, J. M. Ugalde, Y. Wu, J. M. Mercero, T. Heine, K. J. Donald and G. Merino, *Phys. Chem. Chem. Phys.*, 2012, **14**, 14764.
- 17 Z. Cui, V. Vassilev-Galindo, J. Luis Cabellos, E. Osorio, M. Orozco, S. Pan, Y. Ding and G. Merino, *Chem. Commun.*, 2017, **53**, 138–141.
- 18 Y. Pei and X. C. Zeng, *J. Am. Chem. Soc.*, 2008, **130**, 2580–2592.
- 19 Y.-B. Wu, Y. Duan, G. Lu, H.-G. Lu, P. Yang, P. von R. Schleyer, G. Merino, R. Islas and Z.-X. Wang, *Phys. Chem. Chem. Phys.*, 2012, **14**, 14760.
- 20 Z. Wang and P. V. R. Schleyer, *Angew. Chem., Int. Ed.*, 2002, **114**, 4082–4085.
- 21 H.-J. Zhai, A. N. Alexandrova, K. A. Birch, A. I. Boldyrev and L.-S. Wang, *Angew. Chem., Int. Ed.*, 2003, **42**, 6004–6008.
- 22 A. N. Alexandrova, H.-J. Zhai, L.-S. Wang and A. I. Boldyrev, *Inorg. Chem.*, 2004, **43**, 3552–3554.
- 23 P. von Ragué Schleyer and A. I. Boldyrev, *J. Chem. Soc., Chem. Commun.*, 1991, 1536–1538.

- 24 T. N. Gribanova, R. M. Minyaev and V. I. Minkin, *Mendeleev Commun.*, 2002, **12**, 170–172.
- 25 B. B. Averkiev, A. I. Boldyrev, X. Li and L.-S. Wang, *J. Chem. Phys.*, 2006, **125**, 124305.
- 26 S. Nayak, B. Rao, P. Jena, X. Li and L.-S. Wang, *Chem. Phys. Lett.*, 1999, **301**, 379–384.
- 27 S.-D. Li, G.-M. Ren, C.-Q. Miao and Z.-H. Jin, *Angew. Chem., Int. Ed.*, 2004, **43**, 1371–1373.
- 28 X.-M. Zhang, J. Lv, F. Ji, H.-S. Wu, H. Jiao and P. V. R. Schleyer, *J. Am. Chem. Soc.*, 2011, **133**, 4788–4790.
- 29 A. Müller and G. Henkel, *Chem. Commun.*, 1996, 1005–1006.
- 30 S. Li, C. Miao, J. Guo and G. Ren, *J. Am. Chem. Soc.*, 2004, **126**, 16227–16231.
- 31 A. I. Boldyrev, X. Li and L. Wang, *Angew. Chem., Int. Ed.*, 2000, **112**, 3445–3448.
- 32 M. Driess, J. Aust, K. Merz and C. van Wüllen, *Angew. Chem., Int. Ed.*, 1999, **38**, 3677–3680.
- 33 M. Driess, H. Ackermann, J. Aust, K. Merz and C. von Wüllen, *Angew. Chem., Int. Ed.*, 2002, **41**, 450–453.
- 34 C. Romanescu, T. R. Galeev, A. P. Sergeeva, W.-L. Li, L.-S. Wang and A. I. Boldyrev, *J. Organomet. Chem.*, 2012, **721–722**, 148–154.
- 35 C. Romanescu, T. R. Galeev, W.-L. Li, A. I. Boldyrev and L.-S. Wang, *Angew. Chem., Int. Ed.*, 2011, **50**, 9334–9337.
- 36 W. Li, C. Romanescu, T. R. Galeev, Z. A. Piazza, A. I. Boldyrev and L. Wang, *J. Am. Chem. Soc.*, 2012, **134**, 165–168.
- 37 T. R. Galeev, C. Romanescu, W.-L. Li, L.-S. Wang and A. I. Boldyrev, *Angew. Chem., Int. Ed.*, 2012, **51**, 2101–2105.
- 38 T. Heine and G. Merino, *Angew. Chem., Int. Ed.*, 2012, **51**, 4275–4276.
- 39 G. Merino, M. A. Méndez-Rojas, H. I. Beltrán, C. Corminboeuf, T. Heine and A. Vela, *J. Am. Chem. Soc.*, 2004, **126**, 16160–16169.
- 40 G. Merino, M. A. Méndez-Rojas and A. Vela, *J. Am. Chem. Soc.*, 2003, **125**, 6026–6027.
- 41 P. D. Pancharatna, M. A. Méndez-Rojas, G. Merino, A. Vela and R. Hoffmann, *J. Am. Chem. Soc.*, 2004, **126**, 15309–15315.
- 42 X. Wu, Y. Pei and X. C. Zeng, *Nano Lett.*, 2009, **9**, 1577–1582.
- 43 X. Luo, J. Yang, H. Liu, X. Wu, Y. Wang, Y. Ma, S.-H. Wei, X. Gong and H. Xiang, *J. Am. Chem. Soc.*, 2011, **133**, 16285–16290.
- 44 Z. Zhang, X. Liu, B. I. Yakobson and W. Guo, *J. Am. Chem. Soc.*, 2012, **134**, 19326–19329.
- 45 Y. Li, Y. Liao, P. V. R. Schleyer and Z. Chen, *Nanoscale*, 2014, **6**, 10784.
- 46 J. Dai, X. Wu, J. Yang and X. C. Zeng, *J. Phys. Chem. Lett.*, 2014, **5**, 2058–2065.
- 47 C.-S. Liu, H.-H. Zhu, X.-J. Ye and X.-H. Yan, *Nanoscale*, 2017, **9**, 5854–5858.
- 48 Y. Li, Y. Liao and Z. Chen, *Angew. Chem., Int. Ed.*, 2014, **53**, 7248–7252.
- 49 Y. Wang, F. Li, Y. Li and Z. Chen, *Nat. Commun.*, 2016, **7**, 11488.
- 50 L.-J. Zhou, Y.-F. Zhang and L.-M. Wu, *Nano Lett.*, 2013, **13**, 5431–5436.
- 51 L.-M. Yang, I. A. Popov, A. I. Boldyrev, T. Heine, T. Frauenheim and E. Ganz, *Phys. Chem. Chem. Phys.*, 2015, **17**, 17545–17551.
- 52 L.-M. Yang, V. Bačić, I. A. Popov, A. I. Boldyrev, T. Heine, T. Frauenheim and E. Ganz, *J. Am. Chem. Soc.*, 2015, **137**, 2757–2762.
- 53 L.-M. Yang, I. A. Popov, T. Frauenheim, A. I. Boldyrev, T. Heine, V. Bačić and E. Ganz, *Phys. Chem. Chem. Phys.*, 2015, **17**, 26043–26048.
- 54 H. Zhang, Y. Li, J. Hou, K. Tu and Z. Chen, *J. Am. Chem. Soc.*, 2016, **138**, 5644–5651.
- 55 C. Romanescu, T. R. Galeev, W.-L. Li, A. I. Boldyrev and L.-S. Wang, *Acc. Chem. Res.*, 2013, **46**, 350–358.
- 56 L. Z. Zhang, Z. F. Wang, S. X. Du, H.-J. Gao and F. Liu, *Phys. Rev. B: Condens. Matter*, 2014, **90**, 161402.
- 57 H. Zhang, Y. Li, J. Hou, A. Du and Z. Chen, *Nano Lett.*, 2016, **16**, 6124–6129.
- 58 Y. Wang, J. Lv, L. Zhu and Y. Ma, *Phys. Rev. B: Condens. Matter*, 2010, **82**, 94116.
- 59 Y. Wang, M. Miao, J. Lv, L. Zhu, K. Yin, H. Liu and Y. Ma, *J. Chem. Phys.*, 2012, **137**, 224108.
- 60 Y. Wang, J. Lv, L. Zhu and Y. Ma, *Comput. Phys. Commun.*, 2012, **183**, 2063–2070.
- 61 L. Zhu, H. Liu, C. J. Pickard, G. Zou and Y. Ma, *Nat. Chem.*, 2014, **6**, 644–648.
- 62 Y. Li, J. Hao, H. Liu, Y. Li and Y. Ma, *J. Chem. Phys.*, 2014, **140**, 174712.
- 63 H. Wang, J. S. Tse, K. Tanaka, T. Iitaka and Y. Ma, *Proc. Natl. Acad. Sci. U. S. A.*, 2012, **109**, 6463–6466.
- 64 J. Lv, Y. Wang, L. Zhu and Y. Ma, *Phys. Rev. Lett.*, 2011, **106**, 15503.
- 65 L. Zhu, H. Wang, Y. Wang, J. Lv, Y. Ma, Q. Cui, Y. Ma and G. Zou, *Phys. Rev. Lett.*, 2011, **106**, 145501.
- 66 G. Kresse and J. Furthmüller, *Phys. Rev. B: Condens. Matter*, 1996, **54**, 11169–11186.
- 67 G. Kresse and D. Joubert, *Phys. Rev. B: Condens. Matter*, 1999, **59**, 1758–1775.
- 68 J. P. Perdew, K. Burke and M. Ernzerhof, *Phys. Rev. Lett.*, 1996, **77**, 3865–3868.
- 69 A. D. Becke, *Phys. Rev. A*, 1988, **38**, 3098–3100.
- 70 A. Togo and I. Tanaka, *Scr. Mater.*, 2015, **108**, 1–5.
- 71 G. J. Martyna, M. L. Klein and M. Tuckerman, *J. Chem. Phys.*, 1992, **97**, 2635–2643.
- 72 K. Momma and F. Izumi, *J. Appl. Crystallogr.*, 2011, **44**, 1272–1276.
- 73 A. N. Alexandrova, H.-J. Zhai, L.-S. Wang and A. I. Boldyrev, *Inorg. Chem.*, 2004, **43**, 3552–3554.
- 74 B. Wang, S. Yuan, Y. Li, L. Shi and J. Wang, *Nanoscale*, 2017, **9**, 5577–5582.
- 75 A. Molina-Sánchez and L. Wirtz, *Phys. Rev. B: Condens. Matter*, 2011, **84**, 155413.
- 76 A. J. Mannix, X.-F. Zhou, B. Kiraly, J. D. Wood, D. Alducin, B. D. Myers, X. Liu, B. L. Fisher, U. Santiago, J. R. Guest,

- M. J. Yacaman, A. Ponce, A. R. Oganov, M. C. Hersam and N. P. Guisinger, *Science*, 2015, **350**, 1513–1516.
- 77 G. Tai, T. Hu, Y. Zhou, X. Wang, J. Kong, T. Zeng, Y. You and Q. Wang, *Angew. Chem., Int. Ed.*, 2015, **54**, 15473–15477.
- 78 B. Feng, J. Zhang, Q. Zhong, W. Li, S. Li, H. Li, P. Cheng, S. Meng, L. Chen and K. Wu, *Nat. Chem.*, 2016, **8**, 563.
- 79 B. Aufray, A. Kara, S. Vizzini, H. Oughaddou, C. Léandri, B. Ealet and G. Le Lay, *Appl. Phys. Lett.*, 2010, **96**, 183102.
- 80 A. D. Becke and K. E. Edgecombe, *J. Chem. Phys.*, 1990, **92**, 5397–5403.
- 81 G. Henkelman, A. Arnaldsson and H. Jónsson, *Comput. Mater. Sci.*, 2006, **36**, 354–360.
- 82 Y. Jing, Z. Zhou, C. R. Cabrera and Z. Chen, *J. Phys. Chem. C*, 2013, **117**, 25409–25413.
- 83 T. Yu, S. Zhang, F. Li, Z. Zhao, L. Liu, H. Xu and G. Yang, *J. Mater. Chem. A*, 2017, **5**, 18698–18706.
- 84 G. Henkelman, B. P. Uberuaga and H. Jónsson, *J. Chem. Phys.*, 2000, **113**, 9901–9904.
- 85 G. A. Tritsarlis, E. Kaxiras, S. Meng and E. Wang, *Nano Lett.*, 2013, **13**, 2258–2263.